FUNDAMENTAL STEADY-STATE SOLUTION FOR THE TRANSVERSELY ISOTROPIC HALF-SPACE

A. Noorzad

Department of Civil Engineering, Tehran University
Tehran, Iran, soilporous@yahoo.com

M. Eskandari Ghadi

Department of Civil Engineering, Mazandaran University of Science and Technology
Babol, Iran, Ghadi@infopars.net

K. Konagai

Institute of Industrial Science, Tokyo University
Tokyo, Japan, konagai@iis.u-tokyo.ac.jp

(Received: May 2, 2001 - Accepted: August 16, 2002)

Abstract Response of a transversely isotropic 3-D half-space subjected to a surface time-harmonic excitation is presented in analytical form. The derivation of the fundamental solutions expressed in terms of displacements is based on the prefect series of displacement potential functions that have been obtained in the companion paper by the authors. First the governing equations are uncoupled in the cylindrical coordinates. Then, the uncoupled equations are analytically solved to obtain Green functions that are expressed in terms of Fourier series in the tangential direction of the coordinates and in terms of Hankel functions in its radial direction. The analytical Green functions of this paper are exactly same as the results of Lamb (1904) in the case of isotropic material. The Green functions can be used as the kernel functions of the boundary integral equation that is used to solve elastodynamic boundary value problems.

Key Words Transversely Isotropic, Elastodynamic Boundary Value Problem, Time Harmonic, Fundamental Solution (Green Function), Potential Function, Fourier Series

چکیده در این مقاله پاسخ محیط ارتجاعی- خطی با رفتار ایزوتوپ جانبی تحت اثر تحریک سطحی هارمونیک به صورت تحلیلی بدست می‌آید. جواب اساسی (توابع گرین) مساله به صورت توابع تغییر مکان بر اساس توابع پتانسیل ارائه شده در مقاله مکمل به دست می‌آید. بدین منظور، در ابتدا دستگاه معادلات دیفرانسیل حاکم بر مساله در دستگاه مختصات استوانه‌ای به صورت جدا از هم در آمده و سپس معادلات مستقل شده به صورت تحلیلی با استفاده از سری فوریه در امتداد مماسی و تبدیل هنکل در امتداد شعاعی حل می‌شوند. توابع گرین تغییر مکان به دست آمده در این مقاله، در حالت ساده‌تر مربوط به محیط ارتجاعی– خطی با رفتار ایزوتوپ با نتایج لمب که در سال ۱۹۰٤ به دست آورده است، کاملا منطبق می‌باشد. نتایج عددی به منظور نشان دادن شکل تغییر مکان‌ها نیز انطباق خوبی با جواب موجود در محیط ایزوتوپ دارد. توابع گرین این مقاله می‌تواند برای حل مسائل انتشار امواج به روش المان‌های مرزی به عنوان هسته انتگرال‌ها مورد استفاده قرار گیرد.

1. INTRODUCTION

The study of elastic wave propagation was initiated by the pioneering work by Lamb (1904) providing the responses of both two-dimensional and three-dimensional elastic half spaces subject to time-dependent harmonic surface point loads. The response in Lamb's paper is expressed in terms of

displacement vectors. Since then, a number of approaches have been made to solve the problems of wave propagation through an isotropic medium. Using Helmholtz decomposition (Achenbach, 1973), the equations for an isotropic medium are easily uncoupled. Certainly, however, the method does not allow us to cope with the complicated problems of wave propagation through an anisotropic medium. On the other hand, anisotropic materials have been extensively used in engineering practices. In case of soil-structure interaction problems, for example, it is to be noted that soils are mostly viewed as transversely isotropic materials. This fact demands further extensive study on the problems related to the dynamics of these materials.

A transversely isotropic medium is viewed as a particular case of anisotropic materials. Svnge (1957) studied the propagation of Rayleigh waves in a transversely isotropic medium, and proved that the Rayleigh waves propagate only when the stress-free surface of the material is parallel or normal to the axis of symmetry. Freeman and Keer (1972) solved, by using potential functions, the vibratory motion of a body resting on an orthotropic half-plane. Rajapakse and Wang (1991) have also obtained the solution for an embedded body. They first uncoupled the set of equations of motion by a method of elimination, and then solved the fourth order ordinary differential equation. Rajapakse and Wang (1993) described the wave propagation problem in a transversely isotropic medium by using integral transformation method as well as the potential functions.

In this paper the Green functions for a transversely isotropic half-space subjected to a time harmonic surface load are presented in the analytical form. The coupled equations of motion described in terms of displacement components are first uncoupled by means of a prefect series of potential functions, which has been obtained by the authors in the companion paper (Ghadi and Noorzad). Then the partial uncoupled equations for the potential functions are solved analytically.

2. THE GOVERNING EQUATIONS

Let us consider transversely isotropic elastic half-space in a cylindrical coordinate system (r,θ,z). The z-axis of the coordinates is assumed to be normal to the plane of isotropy (r,θ). By ignoring body force, the governing equations of motion are written as (Lekhnitskii. 1981):

$$\frac{\partial \sigma_{rr}}{\partial r}+\frac{1}{r}\frac{\partial \sigma_{\theta r}}{\partial \theta}+\frac{1}{r}(\sigma_{rr}-\sigma_{\theta r})+\frac{\partial \sigma_{zr}}{\partial z}=\rho\frac{\partial^2 U}{\partial t^2}$$

$$\frac{\partial \sigma_{r\theta}}{\partial r}+\frac{1}{r}\frac{\partial \sigma_{\theta\theta}}{\partial \theta}+\frac{2}{r}\sigma_{r\theta}+\frac{\partial \sigma_{z\theta}}{\partial z}=\rho\frac{\partial^2 V}{\partial t^2}$$

$$\frac{\partial \sigma_{rz}}{\partial r}+\frac{1}{r}\frac{\partial \sigma_{\theta z}}{\partial \theta}+\frac{1}{r}\sigma_{rz}+\frac{\partial \sigma_{zz}}{\partial z}=\rho\frac{\partial^2 W}{\partial t^2} \quad (1)$$

where $\sigma_{rr},\sigma_{r\theta},...$ are stress tensor components, U, V and W are displacements in r, θ and z direction, respectively and ρ is the density of the medium.

The strain-stress relationship of the medium is given as (Lekhnitskii. 1981):

$$\begin{bmatrix}\varepsilon_{rr}\\ \varepsilon_{\theta\theta}\\ \varepsilon_{zz}\\ \varepsilon_{rz}\\ \varepsilon_{\theta z}\\ \varepsilon_{r\theta}\end{bmatrix}= \begin{bmatrix} a_{11} & a_{12} & a_{13} & 0 & 0 & 0\\ a_{12} & a_{11} & a_{13} & 0 & 0 & 0\\ a_{13} & a_{13} & a_{13} & 0 & 0 & 0\\ 0 & 0 & 0 & 0.5a_{44} & 0 & 0\\ 0 & 0 & 0 & 0 & 0.5a_{44} & 0\\ 0 & 0 & 0 & 0 & 0 & 0.5a_{66}\end{bmatrix}\begin{bmatrix}\sigma_{rr}\\ \sigma_{\theta\theta}\\ \sigma_{zz}\\ \sigma_{rz}\\ \sigma_{\theta z}\\ \sigma_{r\theta}\end{bmatrix} \quad (2)$$

with

$$a_{66}=2\,(a_{11}-a_{12}) \quad (3)$$

where a_{11}, a_{12},… are the elastic constants.

From Equation 2, stress components are described in terms of strains as:

$$\begin{bmatrix}\sigma_{rr}\\ \sigma_{\theta\theta}\\ \sigma_{zz}\\ \sigma_{rz}\\ \sigma_{\theta z}\\ \sigma_{r\theta}\end{bmatrix}= \begin{bmatrix} A_{11} & A_{12} & A_{13} & 0 & 0 & 0\\ A_{12} & A_{11} & A_{13} & 0 & 0 & 0\\ A_{13} & A_{13} & A_{13} & 0 & 0 & 0\\ 0 & 0 & 0 & 2A_{44} & 0 & 0\\ 0 & 0 & 0 & 0 & 2A_{44} & 0\\ 0 & 0 & 0 & 0 & 0 & 2A_{66}\end{bmatrix}\begin{bmatrix}\varepsilon_{rr}\\ \varepsilon_{\theta\theta}\\ \varepsilon_{zz}\\ \varepsilon_{rz}\\ \varepsilon_{\theta z}\\ \varepsilon_{r\theta}\end{bmatrix} \quad (4)$$

where the coefficients A_{11}, A_{12},… are expressed as:

$$A_{11}=\frac{a_{11}a_{33}-a_{13}^2}{(a_{11}-a_{12})m},\ A_{12}=\frac{a_{13}^2-a_{12}a_{33}}{(a_{11}-a_{12})m},$$
$$A_{13}=-\frac{a_{13}}{m},\ A_{33}=\frac{a_{11}+a_{33}}{m},\ A_{44}=\frac{1}{a_{44}}, \quad (5)$$
$$A_{66}=\frac{1}{a_{66}}$$

with

$$m=(a_{11}+a_{12})a_{33}-2a_{13}^2 \quad (6)$$

Substituting the strain-displacement relationship 151 into Equation 4, the stress components are expressed in terms of the displacements. With the results substituted into Equation 1, the governing equations of motion take the form as following:

$$A_{11}\left(\frac{\partial^2U}{\partial r^2}+\frac{1}{r}\frac{\partial U}{\partial r}-\frac{U}{r^2}\right)+\frac{A_{11}-A_{12}}{2}\frac{1}{r^2}\frac{\partial^2U}{\partial\theta^2}$$
$$+A_{44}\frac{\partial^2U}{\partial z^2}+\frac{A_{11}+A_{12}}{2}\left(\frac{1}{r}\frac{\partial^2V}{\partial r\partial\theta}+\frac{1}{r^2}\frac{\partial V}{\partial\theta}\right)$$
$$-2A_{11}\frac{1}{r^2}\frac{\partial V}{\partial\theta}+(A_{13}+A_{44})\frac{\partial^2W}{\partial r\partial z}=\rho\frac{\partial^2U}{\partial t^2}$$

$$\frac{A_{11}-A_{12}}{2}\left(\frac{\partial^2V}{\partial r^2}+\frac{1}{r}\frac{\partial V}{\partial r}-\frac{V}{r^2}\right)+A_{11}\frac{1}{r^2}\frac{\partial^2V}{\partial\theta^2}$$
$$+A_{44}\frac{\partial^2V}{\partial z^2}+\frac{A_{11}+A_{12}}{2}\left(\frac{1}{r}\frac{\partial^2U}{\partial r\partial\theta}+\frac{1}{r^2}\frac{\partial U}{\partial\theta}\right)$$
$$+2A_{11}\frac{1}{r^2}\frac{\partial U}{\partial\theta}+(A_{13}+A_{44})\frac{\partial^2W}{\partial r\partial z}=\rho\frac{\partial^2V}{\partial t^2}$$

$$A_{44}\left(\frac{\partial^2W}{\partial r^2}+\frac{1}{r}\frac{\partial W}{\partial r}-\frac{W}{r^2}\right)+A_{33}\frac{\partial^2W}{\partial z^2}$$
$$+(A_{13}+A_{44})\left(\frac{\partial^2U}{\partial r\partial z}+\frac{1}{r}\frac{\partial U}{\partial z}+\frac{1}{r}\frac{\partial^2V}{\partial\theta\partial z}\right)=\rho\frac{\partial^2W}{\partial t^2} \quad (7)$$

3. THE GENERAL SOLUTION

The general solutions of Equation 7, in the frequency domain are given as follows:

$$U(r,\theta,z,t)=u(r,\theta,z)e^{i\omega t}$$
$$V(r,\theta,z,t)=v(r,\theta,z)e^{i\omega t} \quad (8)$$
$$W(r,\theta,z,t)=w(r,\theta,z)e^{i\omega t}$$

According to the work by the authors presented in the companion paper (Ghadi and Noorzad), the displacement components in the frequency domain are expressed in terms of scalar potential functions F and χ as:

$$u=-\alpha_3\frac{\partial^2F}{\partial r\partial z}-\frac{1}{r}\frac{\partial\chi}{\partial\theta} \quad (9)$$

$$v=-\alpha_3\frac{1}{r}\frac{\partial^2F}{\partial\theta\partial z}+\frac{\partial\chi}{\partial r} \quad (10)$$

$$w=(1+\alpha_1)\left[\Delta_{r\theta}^2+\beta\frac{\partial^2}{\partial z^2}+\rho_a\omega^2\right]F \quad (11)$$

where

$$\beta=\frac{\alpha_2}{1+\alpha_1} \quad (12)$$

$$\rho_a = \frac{\rho_0}{1+\alpha_1} \qquad \rho_0 = \frac{\rho}{A_{66}} \tag{13}$$

$$\alpha_1 = \frac{A_{66}+A_{12}}{A_{66}},\ \alpha_2 = \frac{A_{44}}{A_{66}},\ \alpha_3 = \frac{A_{13}+A_{44}}{A_{66}} \tag{14}$$

$$\Delta_{r\theta}^2 = \frac{\partial^2}{\partial r^2} + \frac{1}{r}\frac{\partial}{\partial r} + \frac{1}{r^2}\frac{\partial^2}{\partial \theta^2} \tag{15}$$

Substituting Equations 9-11 in Equation 8 yields all the equations of motion (Equation 7) described in terms of the potential functions F and χ. These potential functions are eventually found to satisfy the following equations:

$$\Delta_1^2 \Delta_2^2 F = 0 \tag{16}$$

$$\Delta_0^2 \chi = 0 \tag{17}$$

where

$$\Delta_0^2 = \Delta_{r\theta}^2 + \frac{1}{S_0^2}\frac{\partial^2}{\partial z^2} + \rho\omega^2 \tag{18}$$

$$\Delta_i^2 = \Delta_{r\theta}^2 + \frac{1}{S_i^2}\frac{\partial^2}{\partial z^2} + \frac{1}{\mu_i}\rho\omega^2 \qquad (i=1,2) \tag{19}$$

$$S_0^2 = \frac{1}{\alpha_2} = \frac{A_{66}}{A_{44}} \tag{20}$$

where

$$\mu_1 = \alpha_2 = \frac{A_{44}}{A_{66}} \tag{21}$$

$$\mu_2 = \alpha_1 + 1 = \frac{A_{11}}{A_{66}} \tag{22}$$

S_1^2 and S_2^2 are the roots of the following equation, and are not pure imaginary numbers (Lekhnitskii, 1981):

$$A_{33}A_{44}S^2 + (A_{13}^2 + 2A_{13}A_{44} - A_{11}A_{33})S^2 + A_{11}A_{44} = 0 \tag{23}$$

3.1. Determination of Functions χ and F

For obtaining the functions χ and F, they are expressed herein in the form of Fourier expansion with respect to the circumferential coordinate θ, i.e.

$$\chi(r,\theta,z) = \sum_{m=-\infty}^{+\infty} \chi_m(r,z)e^{i\omega\theta} \tag{24}$$

$$F(r,\theta,z) = \sum_{m=-\infty}^{+\infty} F_m(r,z)e^{i\omega\theta} \tag{25}$$

where χ_m and F_m are respectively the Fourier expansion coefficients of functions F and χ. Substituting Equation 24 in Equation 17 and applying the Hankel transform of order m to χ_m, leads to the following equation

$$\frac{1}{S0}\frac{d^2\chi_m^m}{dz^2} + (\rho_a\omega^2 - \zeta^2)\chi_m^m = 0 \tag{26}$$

where χ_m^m is the (m)th-order Hankel transform of function χ_m^m which is defined as:

$$\chi_m^m(\zeta,z) = \int_0^\infty \chi_m(r,z)rJ_m(\zeta r)dr \tag{27}$$

and the inverse relationship is given by

$$\chi_m(r,z) = \int_0^\infty \chi_m^m(\zeta,z)\zeta J_m(\zeta r)dr \tag{28}$$

where $J_m(\zeta m)$ is the (m)th-order Bessel function of the first kind.

The solution of Equation 26 is

$$\chi_m^m(\zeta,z) = A_m(\zeta)e^{-\alpha_0' z} \tag{29}$$

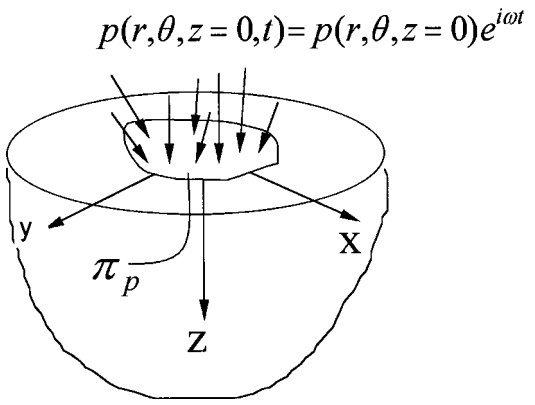

Figure 1. Semi-infinite transversely istropic medium under arbitrary surface harmonic load.

with

$$\alpha_0' = S_0\sqrt{(\rho_a\omega^2 - \zeta^2)} \tag{30}$$

The coefficient $A_m(\zeta)$ is to be determined from the boundary condition. In Equation 29, the term $e^{\alpha_0' z}$ is omitted, because only outwardly propagating waves are considered. The solution of Equation 16 in the wave number domain is

$$F_m^m(\zeta,z) = B_m(\zeta)e^{-\alpha_1' z} + C_m(\zeta)e^{-\alpha_2' z} \tag{31}$$

with

$$\alpha_1' = S_1\sqrt{(\frac{\rho_a}{\mu_1}\omega^2 - \zeta^2)} \tag{32}$$

$$\alpha_2' = S_2\sqrt{(\frac{\rho_a}{\mu_2}\omega^2 - \zeta^2)} \tag{33}$$

where $B_m(\zeta)$ and $C_m(\zeta)$ are arbitrary functions to be determined from the boundary conditions.

3.2. Boundary Conditions It is assumed that a harmonic load is applied to a patch π_p on the stress free surface of the half space (Figure 1). The boundary conditions are expressed in the actual space as:

$$\sigma_{zj}(r,\theta) = p_j(r,\theta) \qquad (r,\theta)\in \pi_p, z=0, (j=r,\theta,z) \tag{34}$$

$$\sigma_{zj}(r,\theta) = 0 \qquad (r,\theta)\notin \pi_p, z=0, (j=r,\theta,z) \tag{35}$$

where $p_j(r,\theta)$ is the (j)th component of the load vector. Expanding the above stress and load functions in Fourier series with respect to θ, the transformed boundary conditions are expressed as:

$$\sigma_{zjm}(r) = p_{jm}(r) \qquad (r)\in \pi_p, z=0, (j=r,\theta,z) \tag{36a}$$

$$\sigma_{zjm}(r) = 0 \qquad (r)\notin \pi_p, z=0, (j=r,\theta,z) \tag{36b}$$

From Equations 30 and 32, Fourier coefficients of the functions χ and F are obtained in the wave number domain. It is thus required for the (m)th Fourier harmonic of the displacement function to be obtained in the wave number domain. To do this, the following four displacement functions u_1, u_2, u_1' and u_2' are introduced here as:

$$\begin{aligned} u_1 &= -\frac{i}{r}\frac{\partial\chi}{\partial\theta} + \frac{\partial X}{\partial r} \\ u_2 &= -\frac{i}{r}\frac{\partial X}{\partial\theta} + \frac{\partial X}{\partial r} \\ u_1' &= -\alpha_3\frac{\partial^2 F}{\partial r\partial z} + \alpha_3 i\frac{\partial^2 F}{r\partial\theta\partial z} \\ u_2' &= -\alpha_3\frac{\partial^2 F}{\partial r\partial z} - \alpha_3 i\frac{\partial^2 F}{r\partial\theta\partial z} \end{aligned} \tag{37}$$

where i^2= -1. Comparing Equation 37 with Equation 9 and 10, it is noted that:

$$\begin{aligned} u &= \frac{1}{2}(u_1' + u_2') - \frac{i}{2}(u_1 - u_2) \\ v &= \frac{1}{2}(u_1 + u_2) + \frac{i}{2}(u_1' - u_2') \end{aligned} \tag{37a}$$

The (m)th Fourier hannonics of the above

TABLE 1. Functions A_m, B_m and C_m in Terms of Load Functions.

Load Components	A_{mj}	B_{mj}	C_{mj}
$p_z = p_\theta = 0, j = r$	$\frac{p_1 i}{2\zeta A_{44}}$	$\frac{a_2 p_2}{2\zeta g(\zeta)}$	$-\frac{a_1 p_2}{2\zeta g(\zeta)}$
$p_z = p_r = 0, j = \theta$	$-\frac{p_4}{2\zeta A_{44}}$	$\frac{a_2 p_3 i}{2\zeta g(\zeta)}$	$-\frac{a_1 p_3 i}{2\zeta g(\zeta)}$
$p_r = p_\theta = 0, j = z$	0	$\frac{c_2 p_2}{g(\zeta)}$	$-\frac{c_1 p_5}{g(\zeta)}$

displacement functions are:

$$\begin{aligned} u_{1m} &= -\frac{i}{r}\frac{\partial X_m}{\partial r} + \frac{m}{r} X_m \chi \\ u_{2m} &= \frac{\partial X_m}{\partial r} - \frac{m}{r} X_m \\ u'_{1m} &= -\alpha_3 \frac{\partial}{\partial z}\left[\frac{\partial F_m}{\partial r} + \frac{m}{r} F_m\right] \\ u'_{2m} &= -\alpha_3 \frac{\partial}{\partial z}\left[\frac{\partial F_m}{\partial r} - \frac{m}{r} F_m\right] \end{aligned} \tag{38}$$

Applying Hankel transform to these equations yields:

$$\begin{aligned} u_{1m}^{m-1} &= \zeta \chi_m^m \\ u_{2m}^{m+1} &= -\zeta X_m^m \\ u'^{m-1}_{1m} &= -\alpha_3 \zeta \frac{dF_m^m}{dz} \\ u'^{m+1}_{2m} &= \alpha_3 \zeta \frac{dF_m^m}{dz} \end{aligned} \tag{39}$$

Obviously, Equations 38 and 39 show that the Fourier series of the displacement functions u_{1m}, u_{2m}, u'_{1m} and u'_{2m} are described in terms of the inverse transform of χ_m^m and F_m^m. And from Equation 37a the mth Fourier series of the displacement components are found to satisfy the following equations:

$$u_m = \frac{1}{2}(u'_{1m} + u'_{2m}) - \frac{i}{2}(u_{1m} + u_{2m}) \tag{40}$$

$$v_m = \frac{1}{2}(u_{1m} + u_{2m}) + \frac{i}{2}(u'_{1m} - u'_{2m}) \tag{41}$$

Therefore, u_m and v_m are eventually expressed in terms of χ_m^m and F_m^m as:

$$\begin{aligned} u_m = \frac{\alpha_3}{2}\frac{\partial}{\partial z}\Bigg(\int_0^\infty [J_{m+1}(\zeta r) - J_{m-1}(\zeta r)]\zeta^2 F_m^m(\zeta, z)d\zeta\Bigg) \\ -\frac{i}{2}\int_0^\infty [J_{m+1}(\zeta r) + J_{m-1}(\zeta r)]\zeta^2 X_m^m(\zeta r)d\zeta \end{aligned} \tag{42}$$

$$\begin{aligned} u_m = -\alpha_3 \frac{i}{2}\frac{\partial}{\partial z}\Bigg(\int_0^\infty [J_{m+1}(\zeta r) + J_{m-1}(\zeta r)]\zeta^2 F_m^m(\zeta, z)d\zeta\Bigg) \\ -\frac{1}{2}\int_0^\infty [J_{m+1}(\zeta r) - J_{m-1}(\zeta r)]\zeta^2 X_m^m(\zeta r)d\zeta \end{aligned} \tag{43}$$

Likewise, the (m)th Fourier series of the displacement component w is given as:

$$\begin{aligned} w_m = (1+\alpha_1) \\ \int_0^\infty \left[\left(\frac{\rho_0 \omega^2}{1+\alpha_1} - \zeta^2\right) + \frac{\alpha_2}{1+\alpha_1}\frac{d^2}{dz^2}\right] F_m^m J_m(\zeta r)d\zeta \end{aligned} \tag{44}$$

Similarly, for stress components, the following equations are obtained:

$$\begin{aligned} \sigma_{zrm}^{m+1} + i\sigma_{z\theta m}^{m+1} = iA_{44}\frac{d}{dz}\left[-\zeta X_m^m - i\alpha_3 \zeta \frac{dF_m^m}{dz}\right] \\ + A_{44}\left[-\zeta(1+\alpha_1)\left(\frac{\rho_0 \omega^2}{1+\alpha_1} - \zeta^2 + \frac{\alpha_2}{1+\alpha_1}\frac{d^2}{dz^2}\right)F_m^m\right] \end{aligned} \tag{45}$$

$$\begin{aligned} \sigma_{zrm}^{m-1} - i\sigma_{z\theta m}^{m-1} = -iA_{44}\frac{d}{dz}\left[\zeta X_m^m - i\alpha_3 \zeta \frac{dF_m^m}{dz}\right] \\ + A_{44}\left[\zeta(1+\alpha_1)\left(\frac{\rho_0 \omega^2}{1+\alpha_1} - \zeta^2 + \frac{\alpha_2}{1+\alpha_1}\frac{d^2}{dz^2}\right)F_m^m\right] \end{aligned} \tag{46}$$

$$\sigma^{m}_{zzm} = \alpha_3 A_{13} \frac{d}{dz}(-\zeta^2 F^m_m) + A_{33} \frac{d}{dz}(1+\alpha_1)\left(\frac{\rho_0 \omega^2}{1+\alpha_1} - \zeta^2 + \frac{\alpha_2}{1+\alpha_1}\frac{d^2}{dz^2}\right)F^m_m \quad (47)$$

where σ^{j}_{zrm}, $\sigma^{j}_{z\theta m}$ and σ^{j}_{zzm} are the jth order Hankel transform of the mth Fourier series of σ^{j}_{zrm}, $\sigma^{j}_{z\theta m}$ and σ^{j}_{zzm}, respectively. The boundary conditions Equations 36a,b, when Hankel transformed with respect to r, determines the unknown constants A_m, B_m and C_m in Equations 45, 46 and 47. They are listed for different load functions in Table 1.

In Table 1:

$$P(r,\theta) = p_r(r,\theta)e_r + p_\theta(r,\theta)e_\theta + p_z(r,\theta)e_z \quad (48)$$

$$\begin{aligned} p_1 &= p^{m+1}_{rm} + p^{m-1}_{rm} \\ p_2 &= p^{m+1}_{rm} - p^{m-1}_{rm} \\ p_3 &= p^{m+1}_{\theta m} + p^{m-1}_{\theta m} \\ p_4 &= p^{m+1}_{\theta m} - p^{m-1}_{\theta m} \\ p_5 &= p^{m}_{zm} \end{aligned} \quad (49)$$

$$\begin{aligned} a_1 &= \alpha_1' a + \alpha_2 \alpha_1'^3 A_{33} \\ a_2 &= \alpha_2' a + \alpha_2 \alpha_2'^3 A_{33} \\ a &= \alpha_3 A_{13}\zeta^2 - A_{13}(1+\alpha_1)\zeta^2 + A_{33}\rho_a\omega^2 \\ c_1 &= \alpha_1'\alpha_3 + \rho_a\omega^2 - \zeta^2(1+\alpha_1) + \alpha_1'^2\alpha_2 \\ c_2 &= \alpha_2'\alpha_3 + \rho_a\omega^2 - \zeta^2(1+\alpha_1) + \alpha_2'^2\alpha_2 \\ g(\zeta) &= c_2 a_1 - c_1 a_2 \\ a_1 &= \alpha_1' a + \alpha_2 \alpha_1'^3 A_{33} \end{aligned} \quad (50)$$

4. GREEN FUNCTIONS

Substituting A_m, B_m and C_m from Table 1 into Equations 42 to 45, the m(th) Fourier series of the displacement Green functions are obtained as

$$G_{rrm} = \frac{\alpha_3}{2}\int_0^\infty \zeta[J_{m+1}(\zeta r) - J_{m-1}(\zeta r)]\left[\alpha_1\alpha_2' e^{-\alpha_2' z} - \alpha_2\alpha_1' e^{-\alpha_1' z}\right] \frac{p_2}{2A_{44}}\frac{d\zeta}{g(\zeta)} - \frac{1}{2}\int_0^\infty \zeta[J_{m+1}(\zeta r) + J_{m-1}(\zeta r)]\frac{p_1}{2A_{44}\alpha_0'} e^{-\alpha_0' z} d\zeta \quad (51)$$

$$G_{\theta rm} = -i\frac{\alpha_3}{2}\int_0^\infty \zeta[J_{m+1}(\zeta r) - J_{m-1}(\zeta r)]\left[\alpha_1\alpha_2' e^{-\alpha_2' z} - \alpha_2\alpha_1' e^{-\alpha_1' z}\right] \frac{p_2}{2A_{44}}\frac{d\zeta}{g(\zeta)} + \frac{i}{2}\int_0^\infty \zeta[J_{m+1}(\zeta r) - J_{m-1}(\zeta r)]\frac{p_1}{2A_{44}\alpha_0'} e^{-\alpha_0' z} d\zeta \quad (52)$$

$$G_{zrm} = \int_0^\infty \left(\left[\rho_a\omega^2 - \zeta(1+\alpha_1)\right]\left[\alpha_2 e^{-\alpha_1' z} - \alpha_1 e^{-\alpha_2' z}\right] + \alpha_2\left[\alpha_2\alpha_1'^2 e^{-\alpha_1' z} - \alpha_1\alpha_2'^2 e^{-\alpha_2' z}\right]\frac{p_2}{2A_{44}} J_m(\zeta r)\frac{d\zeta}{g(\zeta)} \right) \quad (53)$$

$$G_{r\theta m} = i\frac{\alpha_3}{2}\int_0^\infty \zeta[J_{m+1}(\zeta r) - J_{m-1}(\zeta r)]\left[\alpha_1\alpha_2' e^{-\alpha_2' z} - \alpha_2\alpha_1' e^{-\alpha_1' z}\right] \frac{p_3}{2A_{44}}\frac{d\zeta}{g(\zeta)} - \frac{i}{2}\int_0^\infty \zeta[J_{m+1}(\zeta r) + J_{m-1}(\zeta r)]\frac{p_4}{2A_{44}\alpha_0'} e^{-\alpha_0' z} d\zeta \quad (54)$$

$$G_{rrm} = \frac{\alpha_3}{2}\int_0^\infty \zeta[J_{m+1}(\zeta r) - J_{m-1}(\zeta r)]\left[\alpha_1\alpha_2' e^{-\alpha_2' z} - \alpha_2\alpha_1' e^{-\alpha_1' z}\right] \frac{p_2}{2A_{44}}\frac{d\zeta}{g(\zeta)} - \frac{1}{2}\int_0^\infty \zeta[J_{m+1}(\zeta r) + J_{m-1}(\zeta r)]\frac{p_1}{2A_{44}\alpha_0'} e^{-\alpha_0' z} d\zeta \quad (55)$$

$$G_{rrm} = \frac{\alpha_3}{2}\int_0^\infty \zeta[J_{m+1}(\zeta r) - J_{m-1}(\zeta r)]\left[\alpha_1\alpha_2' e^{-\alpha_2' z} - \alpha_2\alpha_1' e^{-\alpha_1' z}\right] \frac{p_2}{2A_{44}}\frac{d\zeta}{g(\zeta)} - \frac{1}{2}\int_0^\infty \zeta[J_{m+1}(\zeta r) + J_{m-1}(\zeta r)]\frac{p_1}{2A_{44}\alpha_0'} e^{-\alpha_0' z} d\zeta \quad (56)$$

$$G_{rrm} = \frac{\alpha_3}{2}\int_0^\infty \zeta[J_{m+1}(\zeta r) - J_{m-1}(\zeta r)]\left[\alpha_1\alpha_2' e^{-\alpha_2' z} - \alpha_2\alpha_1' e^{-\alpha_1' z}\right] \frac{p_2}{2A_{44}}\frac{d\zeta}{g(\zeta)} - \frac{1}{2}\int_0^\infty \zeta[J_{m+1}(\zeta r) + J_{m-1}(\zeta r)]\frac{p_1}{2A_{44}\alpha_0'} e^{-\alpha_0' z} d\zeta \quad (57)$$

TABLE 2. Material Constants.

Material	$\frac{A_{11}}{A_{44}}$	$\frac{A_{12}}{A_{44}}$	$\frac{A_{13}}{A_{44}}$	$\frac{A_{33}}{A_{44}}$	$A_{44}\times 10^4 \frac{N}{mm^2}$
Isotropic	3.00	1.00	1.00	3.00	1.00
Layered soil	2.11	0.43	0.47	2.58	1.40
Beryl rock	4.13	1.47	1.01	3.62	1.00
E-composite	3.17	1.40	11.11	10.04	0.47
G-composite	2.024	0.683	0.073	21.17	0.41

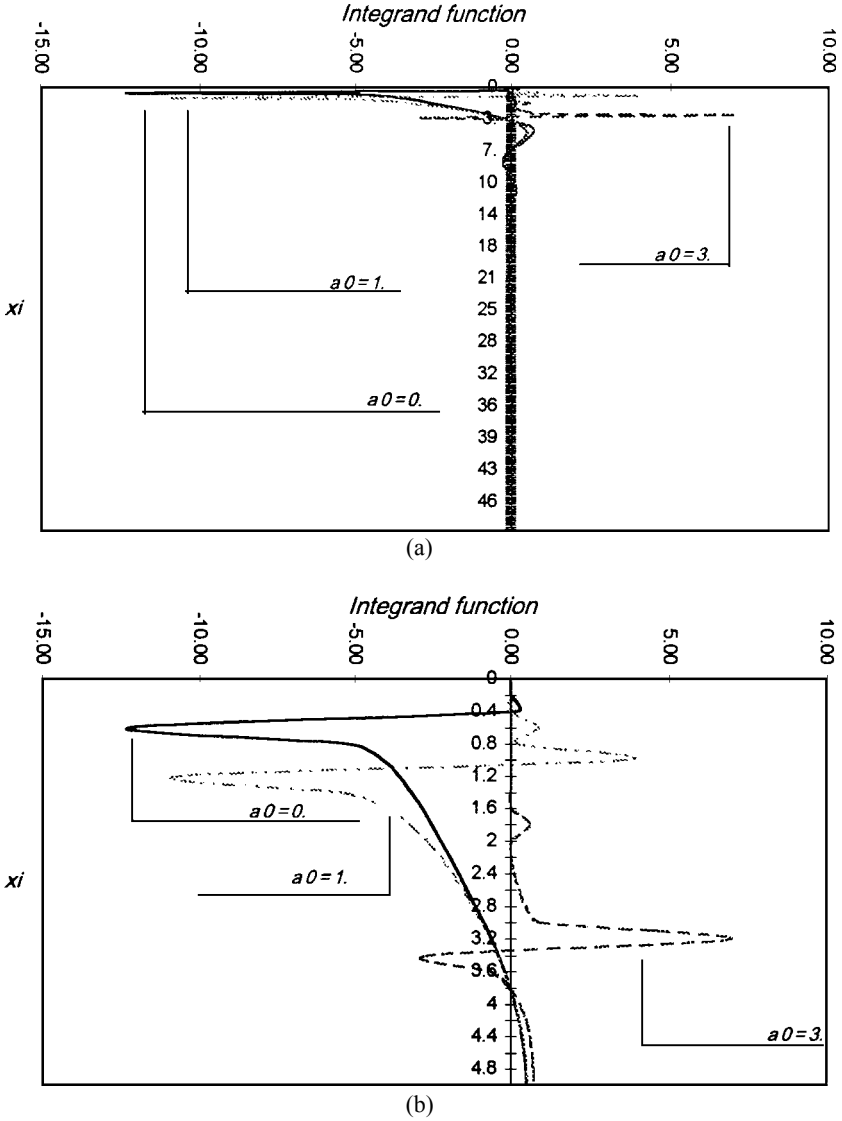

Figure 2. (a), (b) Integrand function of G_{zz} due to uniform patch load of radius R in z-direction (real part, isotropic madium).

$$G_{rrm}=\frac{\alpha_3}{2}\int_0^{\infty}\zeta\left[J_{m+1}(\zeta r)-J_{m-1}(\zeta r)\right]\left[\alpha_1\alpha_2' e^{-\alpha_2' z}-\alpha_2\alpha_1' e^{-\alpha_1' z}\right]\frac{p_2}{2A_{44}}\frac{d\zeta}{g(\zeta)}-\frac{1}{2}\int_0^{\infty}\zeta\left[J_{m+1}(\zeta r)+J_{m-1}(\zeta r)\right]\frac{p_1}{2A_{44}\alpha_0'}e^{-\alpha_0' z}d\zeta \quad (58)$$

$$G_{rrm}=\frac{\alpha_3}{2}\int_0^{\infty}\zeta\left[J_{m+1}(\zeta r)-J_{m-1}(\zeta r)\right]\left[\alpha_1\alpha_2' e^{-\alpha_2' z}-\alpha_2\alpha_1' e^{-\alpha_1' z}\right]\frac{p_2}{2A_{44}}\frac{d\zeta}{g(\zeta)}-\frac{1}{2}\int_0^{\infty}\zeta\left[J_{m+1}(\zeta r)+J_{m-1}(\zeta r)\right]\frac{p_1}{2A_{44}\alpha_0'}e^{-\alpha_0' z}d\zeta \quad (59)$$

4.1. Derivation of the Green Function for the Isotropic Media The Green functions G_{rzm}, $G_{\theta zm}$ and G_{zzm}, Equations 57, 58 and 59, should be identical to those for the isotropic medium subjected to normal point loads P_z when the elastic constants A_{ij} are expressed in terms of Lame constants ((λ,μ)) as following:

$$\begin{aligned} A_{11}&=A_{33}=\lambda+2\mu\\ A_{11}&=A_{33}=\lambda\\ A_{11}&=A_{33}=\mu \end{aligned} \quad (60)$$

Substituting Equation 60 in Equations 57, 58 and 59 yields the following expressions of the Green functions, that are found completely identical to those derived by Lamb (1904), and thus, validating the present approach:

$$\begin{aligned} G_{zz}&=-\frac{p_z}{2\pi\mu}\int_0^{\infty}k^2\,\zeta\alpha\,\frac{J_0(\zeta r)}{F(\zeta)}\,d\zeta\\ G_{rz}&=\frac{p_z}{2\pi\mu}\int_0^{\infty}\frac{\zeta^2\left[2\zeta^2-k^2-2\alpha\beta\right]}{F(\zeta)}J_1(\zeta r)\,d\zeta\\ G_{\theta z}&=0 \end{aligned} \quad (61)$$

where

$$F(\zeta)=-\frac{\mu}{\alpha(\lambda+\mu)^2}g(\zeta)=(2\zeta^2-k^2)-4\zeta^2\alpha\beta \quad (62)$$

$$k^2=\frac{\rho}{\mu}\omega^2 \quad (63)$$

$$\begin{aligned} \alpha^2&=\zeta^2-\frac{\rho}{\lambda+2\mu}\omega^2\\ \beta^2&=\zeta^2-k^2 \end{aligned} \quad (64)$$

5. NUMERICAL RESULTS

The actual values of the Green functions are obtained through numerical evaluation of the integrals with infinite upper limits. The integrands of these integrals are complex functions including Bessel functions with oscillatory features. Bessel functions converge slowly to zero as the variable of integration ζr increases. It is, however, noted that there exist singular points of the integrals, the poles related to Rayliegh wave generation.

These integrals cannot be evaluated analytically even in the case of isotropic medium cases. It is therefore required to employ a suitable numerical scheme to evaluate these Green functions. The singularities and oscillatory nature of the integrand require careful consideration in constructing the integration scheme and in setting the increment of variable of integration as well as the upper limit of the integral at some appropriate values. Reviewing the oscillatory nature of different Green functions, the trapezoidal method is used as the main scheme for numerical integration with the increment of $\Delta\zeta$ set at a particular value less than 0.2. The upper limit of the various integrals have been determined reviewing the characteristics of integrands for different frequencies, ω. Because of the decaying functions $e^{-i\alpha' z}$, (i= 0,1,2), the deeper the point is located, as is included in the integrand, the faster is the convergence.

Numerical evaluations of the integrals have been made assuming that a uniform patch load P_0 of radius R is applied. The obtained Green functions are described herein in terms of non-dimensionalized parameter, including $G_{ij}(=\frac{G_{ij}A_{66}}{P_0R})$, $a_0(=R\omega\sqrt{\frac{\rho}{A_{66}}})$, $\frac{x}{R}$ and $\frac{z}{R}$.

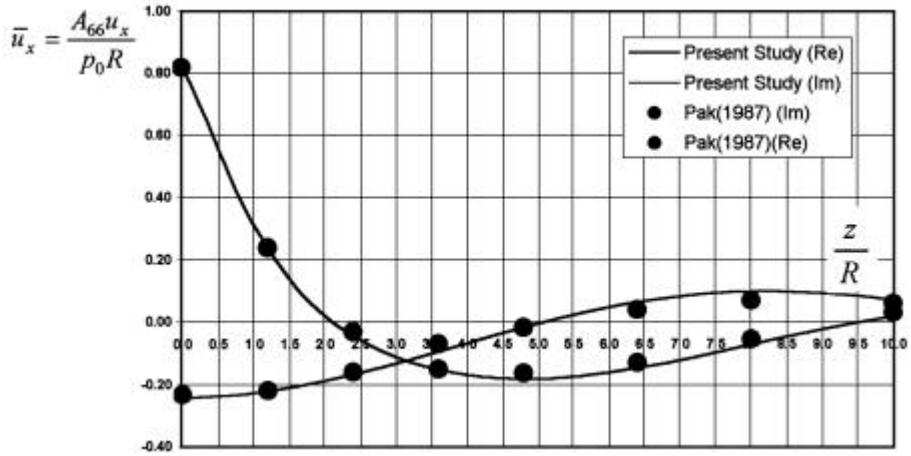

Figure 3. Comparison of displacement in x-direction of isotropic elastic half- space due to uniform patch load of radius R in x-direction.

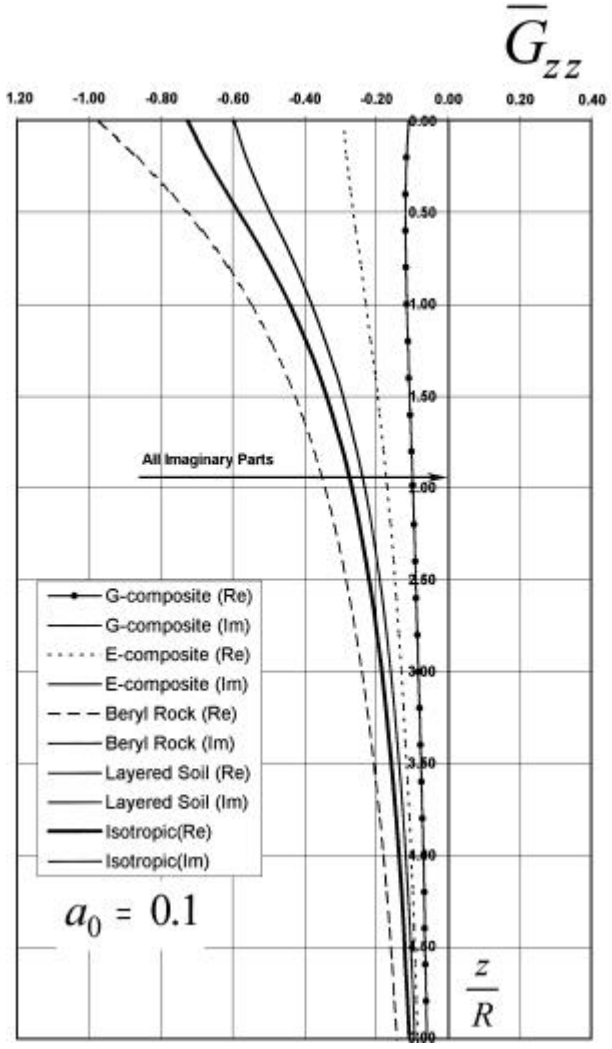

Figure 4. Displacement Green function $\overline{G}_{zz}$ due to uniform patch load of rsdiuc R in z-direction.

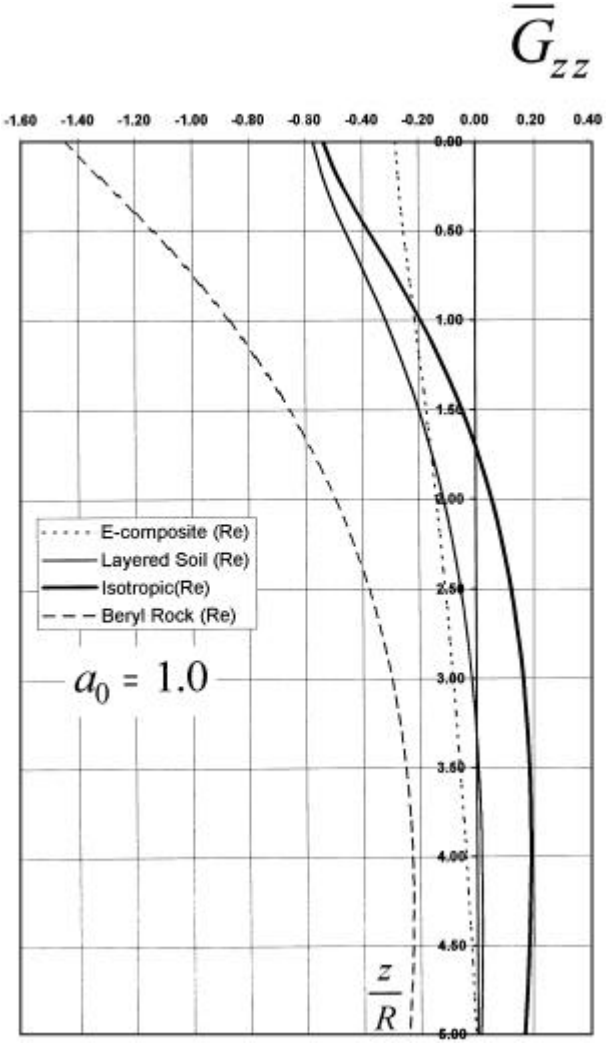

Figure 5. Displacement Green function $\overline{G}_{zz}$ due to uniform patch load of rsdiuc R in z-direction.

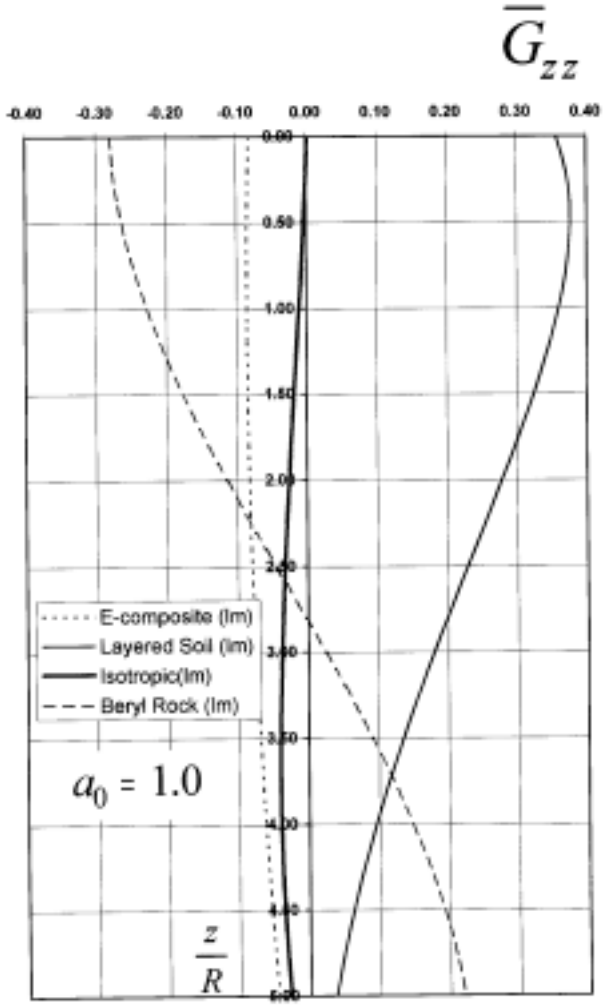

Figure 6. Displacement Green function $\overline{G}_{zz}$ due to uniform patch load of rsdiuc R in z-direction.

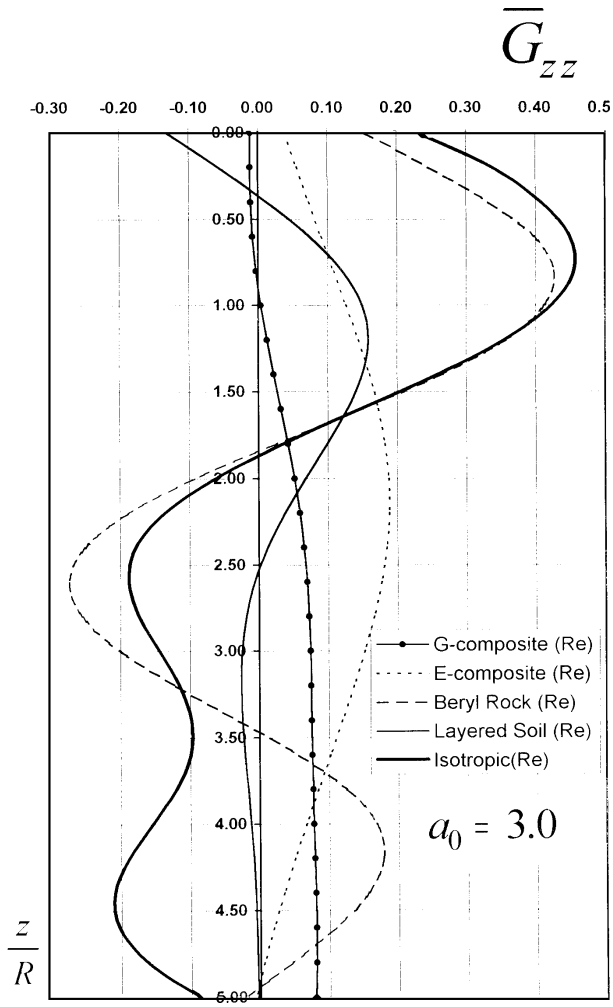

Figure 7. Displacement Green function $\overline{G}_{zz}$ due to uniform patch load of rsdiuc R in z-direction.

The real parts of the integrands for the Green function G_{zz}, for an isotropic medium are plotted for different frequencies a_0= 0.5, 1.0 and 3.0 (Figure 2). This figure clearly shows both singularities and oscillatory nature of the integrands. Singular points of the integrands are different for different frequencies, indicating that the Rayleigh waves propagate with special velocity. Also, this seen that the absolute values of the integrands converge on zero as ζ increases.

Figure 3 shows the variation of u_x for the isotropic material with respect to depth $\frac{z}{R}$. The obtained variation is compared with the numerical solution by Pak (1987). The present solution is in good agreement with that by Pak.

The mechanical features of the different transversely isotropic media (Table 2) are discussed in terms of the present Green functions. These materials are (1) isotropic medium, (2) limestone/sandstone layered soil, (3) Beryl rock, (4) E glass/epoxy composite and (5) Graphite/epoxy composite [7]. The Poisson's ratio of the isotropic material is equal to 0.25.

The graphical results are shown in Figures 4 to 24. According to the figures the following results are worth to mention:

1. The selected algorithm is appropriate for both low and high frequency time-harmonic

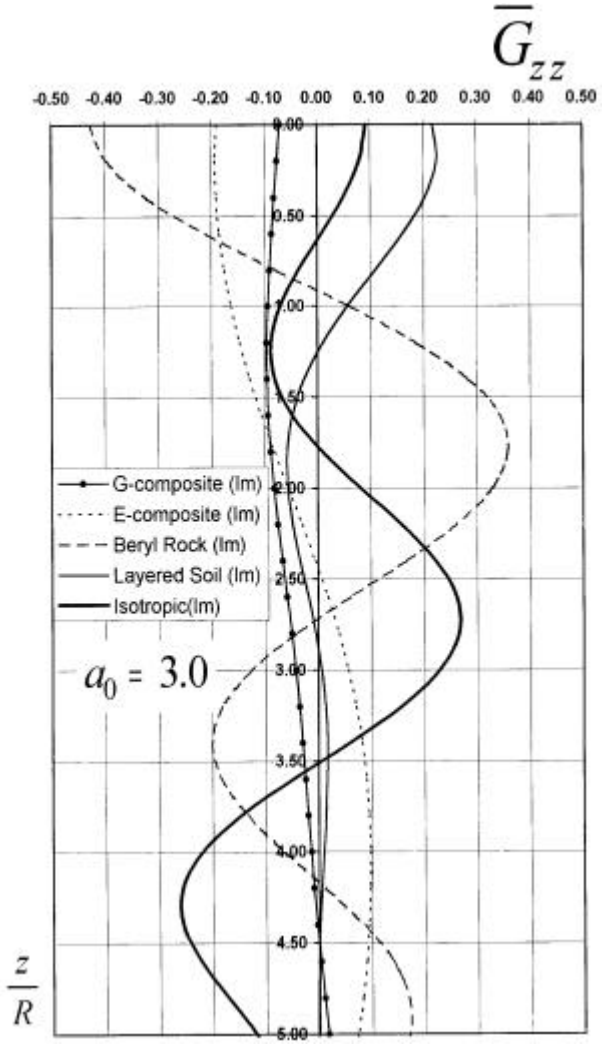

Figure 8. Displacement Green function $\overline{G}_{zz}$ due to uniform patch load of rsdiuc R in z-direction.

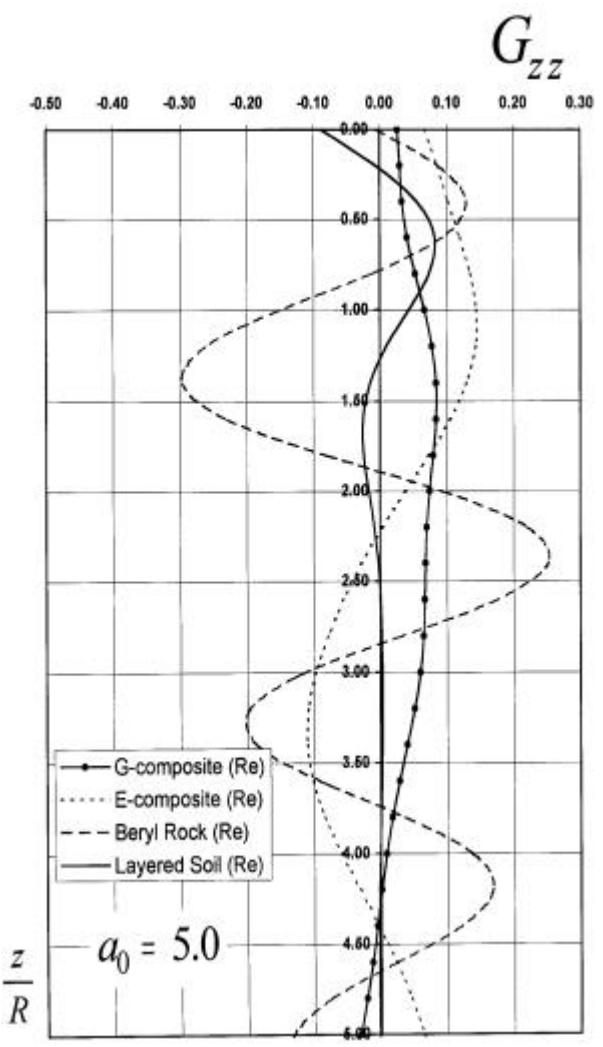

Figure 9. Displacement Green function $\overline{G}_{zz}$ due to uniform patch load of rsdiuc R in z-direction.

motions in all directions (Figures 4 to 22).

2. The imaeinarv parts of the Green functions are identically equal to zero in the case of the equivalently static loads (Figures 4, 11 and 16). In these cases, the differences in the response of the various materials arc dependent on the variation of the material constants.
3. The responses G_{xx} are approximately equal to each other in the case of low frequencies (Figure 16), whereas in the cases of high frequencies the responses are quit different. This result shows that the consideration of the anisotropic mechanical properties is needed. Differences in time-harmonic motion in high frequencies are seen in Figures 17 to 22.
4. By consideration of the figures, it is understood that the wave-number varies almost linearly with respect to the frequency.
5. The wavelength in each direction is directly dependent to the mechanical constant of the same direction. Based on this, it is expected that the wavelength for greater constant is larger than that of the smaller constant. This fact is particularly evident in function G_{zz}. (note that to the differences in A_{33}). See Figures 5 to 15.
6. The decay of displacements with distance is smoother in low frequencies. However, this decay becomes increasingly oscillatory as frequency of loading increases.

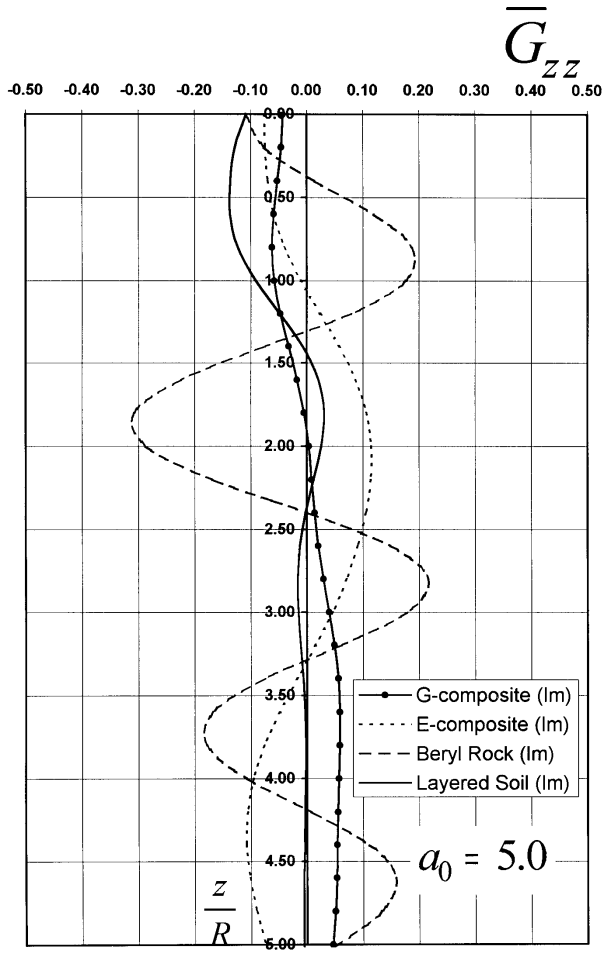

Figure 10. Displacement Green function $\overline{G}_{zz}$ due to uniform patch load of rsdiuc R in z-direction.

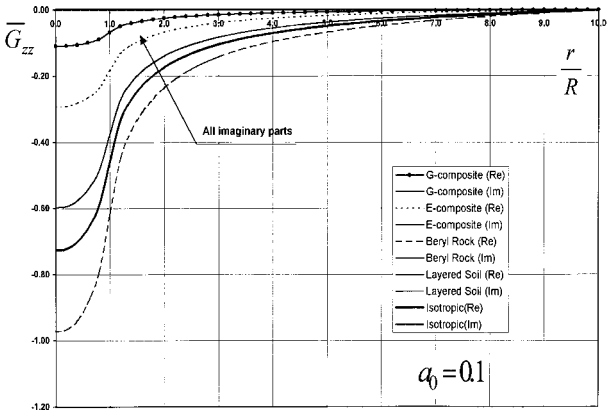

Figure 11. Displacement Green function $\overline{G}_{zz}$ due to uniform patch load of rsdiuc R in z-direction.

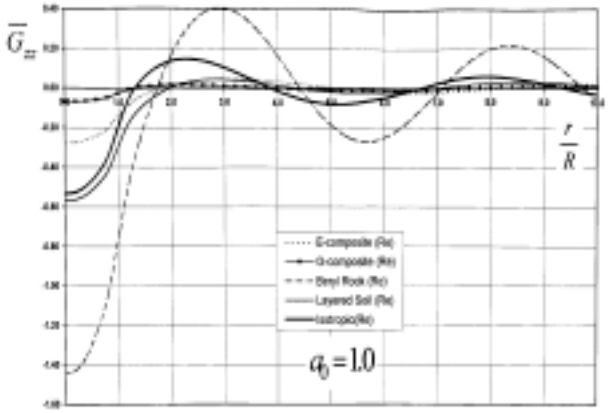

Figure 12. Displacement Green function $\overline{G}_{zz}$ due to uniform patch load of rsdiuc R in z-direction.

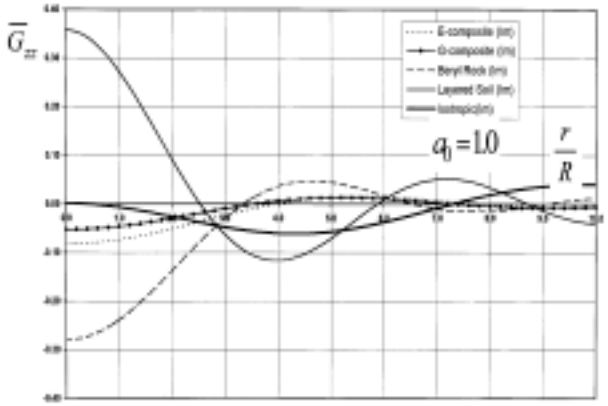

Figure 13. Displacement Green function $\overline{G}_{zz}$ due to uniform patch load of rsdiuc R in z-direction.

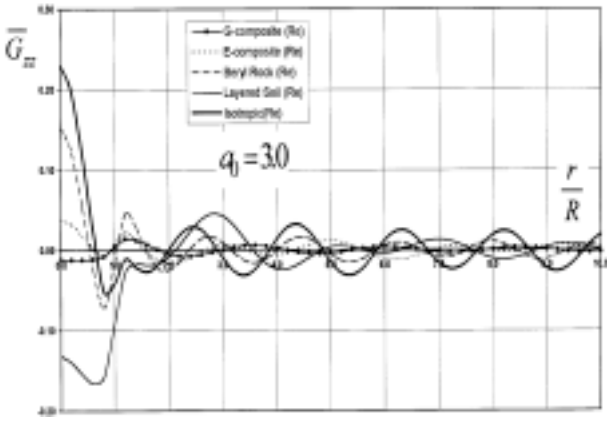

Figure 14. Displacement Green function $\overline{G}_{zz}$ due to uniform patch load of rsdiuc R in z-direction.

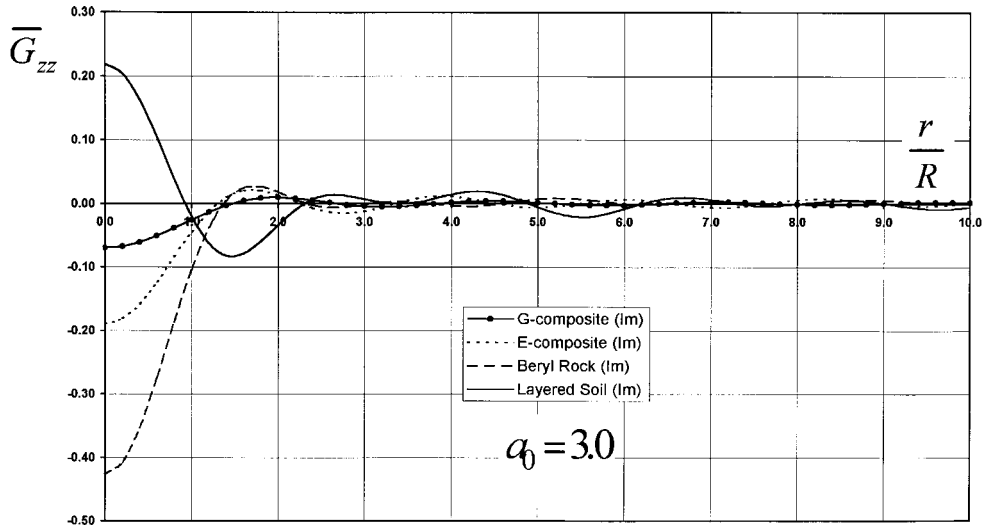

Figure 15. Displacement Green function $\overline{G}_{zz}$ due to uniform patch load of rsdiuc R in z-direction.

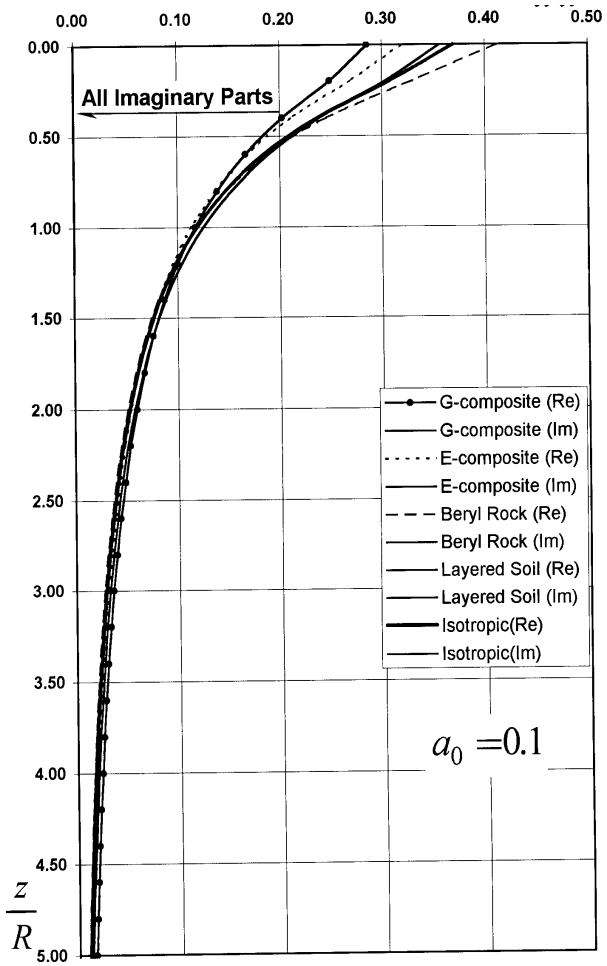

Figure 16. Displacement Green function $\overline{G}_{zz}$ due to uniform patch load of rsdiuc R in z-direction.

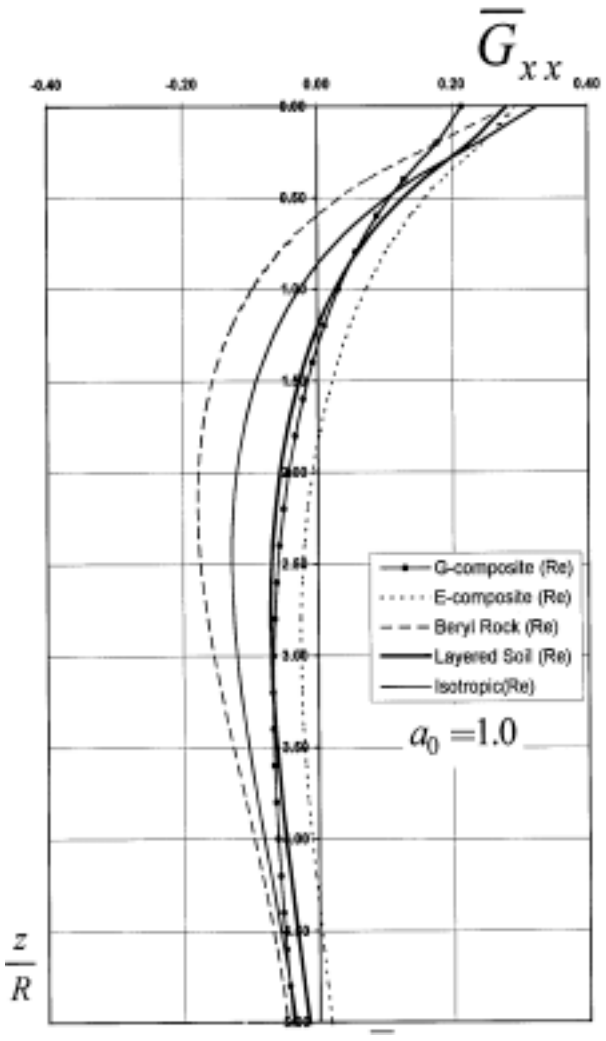

Figure 17. Displacement Green function $\overline{G}_{zz}$ due to uniform patch load of rsdiuc R in z-direction.

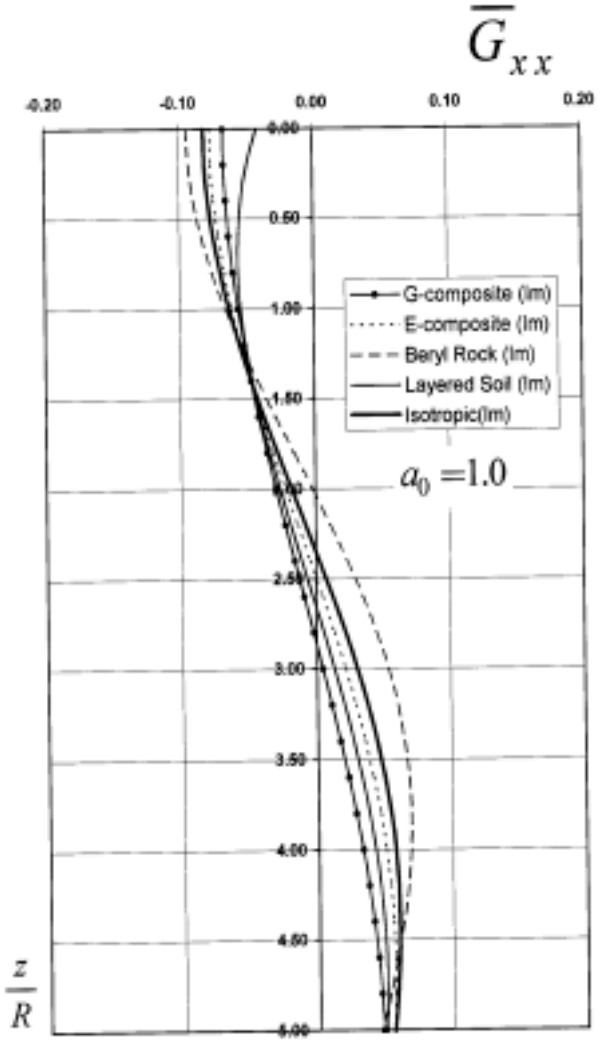

Figure 18. Displacement Green function $\overline{G}_{zz}$ due to uniform patch load of rsdiuc R in z-direction.

6. CONCLUSIONS

Exact displacement Green functions for analytical solution of transversely isotropic elastic half-space subjected to arbitrary time-dependent harmonic surface loadings have been presented. By means of these Green functions analytical solutions have been obtained in wave number domain so that in actual domain, they are in the form of semi-infinite integrals. The integrands of these integrals have a finite number of singularities. For numerical be results, five different materials have used, where one of which is isotropic and the others are transversely isotropic. In numerical evaluation the loads are considered to be uniform patch load of radius R.

According to the numerical results, the influence of material anisotropy on the response G_{xx} and G_{zz} in the case of low frequency is mainly reflected by the values of material constants of that direction i.e. A_{11} and A_{33}, respectively. And, in high frequency, the influence of material

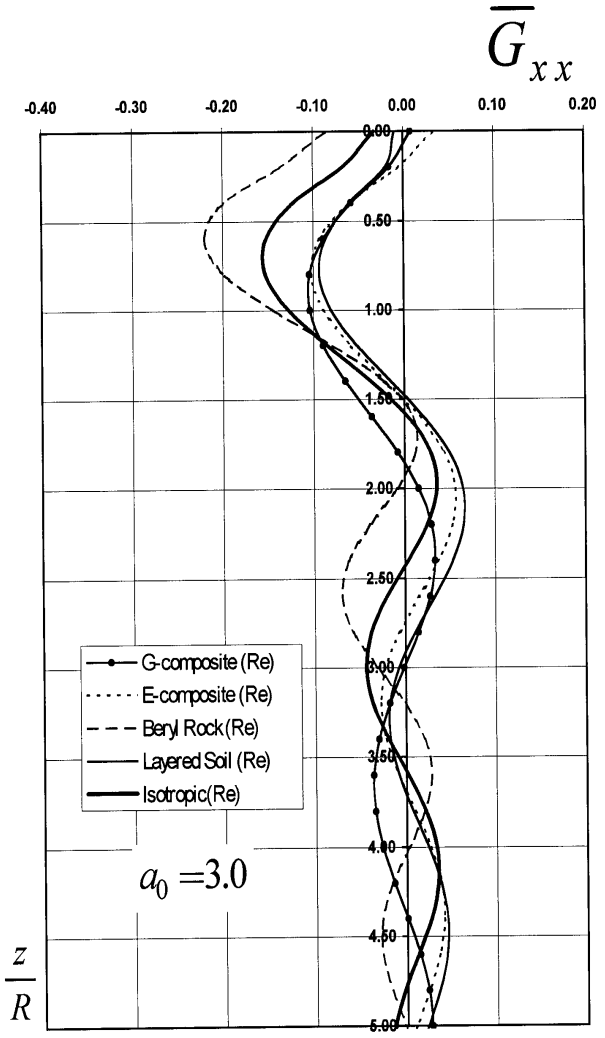

Figure 19. Displacement Green function $\overline{G}_{zz}$ due to uniform patch load of rsdiuc R in z-direction.

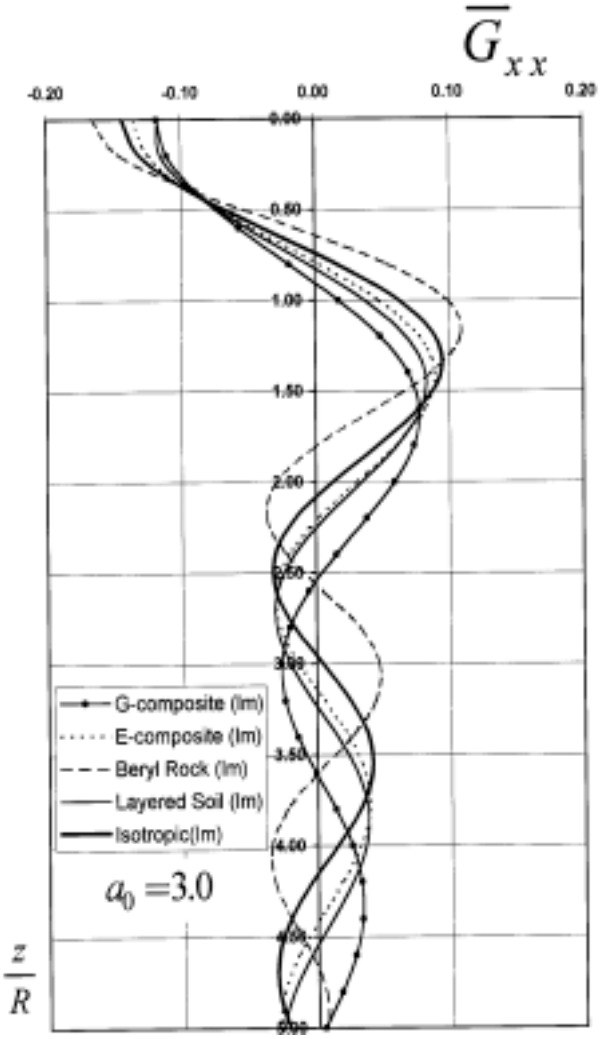

Figure 20. Displacement Green function $\overline{G}_{zz}$ due to uniform patch load of rsdiuc R in z-direction.

anisotropy is reflected not only by the material constant values of that direction but by other material constants as well. The decay of displacements with distance is smoother in low frequencies. However, the decay is turned to be oscillatory in nature as the frequency of loading increases.

These results can be used to develop analytical solutions for some fundamental problems related to earthquake engineering and soil dynamics. Green functions presented in this paper are important in the development of boundary integral equation methods for analysis of seismic wave scattering in transversely isotropic soils and anisotropic soil-structure interaction problems.

7. ACKNOWLEDGMENTS

The authors would like to express their best thanks to Mr. Raquib AHSAN who has kindly taken the trouble in polishing English of this paper.